# Analysis of dense gas effects in compressible turbulent channel flows

L. Sciacovelli, P. Cinnella, and X. Gloerfelt

## 1 Introduction

In this work we investigate the influence of dense gas effects on compressible wall-bounded turbulence. Turbulent flows of dense gases represent a research field of great importance for a wide range of applications in engineering. Dense gases are single-phase fluids with a molecular complexity such that the fundamental derivative of gas dynamics [1] $\Gamma := 1 + \frac{\rho}{c}\left.\frac{\partial c}{\partial \rho}\right|_s$ (where $\rho$ is the density, $p$ the pressure, $s$ the entropy, and $c$ the sound speed), which measures the rate of change of the sound speed in isentropic transformations, is less than one in a range of thermodynamic conditions close to the saturation curve. In such conditions, the speed of sound increases in isentropic expansions and decreases in isentropic compressions, unlike the case of perfect gases. For dense gases, the perfect gas model is no longer valid, and more complex equations of state must be used to account for their peculiar thermodynamic behavior. Moreover, in the dense gas regime, the dynamic viscosity $\mu$ and the thermal conductivity $\lambda$ depend on temperature and pressure through complex relationships. Similarly, the approximation of nearly constant Prandtl number $Pr{=}\mu c_p/\lambda$ is no longer valid. Numerical simulations of turbulent dense gas flows of engineering interest are based on the (Reynolds-Averaged Navier–Stokes) RANS equations, which need to be supplemented by a model for the Reynolds stress tensor and turbulent heat flux. The accuracy of RANS models for dense-gas flows has not been properly assessed up to date, due to the lack of both experimental and numerical reference data. DNS databases [2, 3] are then needed to quantify the deficiencies of existing turbulence models and to develop and calibrate improved ones. In this work we first summarize some recent direct numerical simulation (DNS) results [4] for supersonic turbulent channel flows (TCF) of PP11, a heavy fluorocarbon representative of dense gases, at various bulk Mach and Reynolds numbers. The most relevant effects are represented by non-conventional variations of the fluctuating thermodynamic quantities, compared to perfect gases and a strong decoupling between thermal and dynamic effects almost everywhere in the flow, except in the immediate vicinity of the solid wall. Preliminary considerations about the validity

P. Cinnella · X. Gloerfelt
Laboratoire DynFluid, Arts et Métiers ParisTech, e-mail: {name.surname}@ensam.eu
· L. Sciacovelli
California Institute of Technology, Pasadena, e-mail: lsciacov@caltech.edu

of some currently-used models for the turbulent stresses and heat flux are carried out based on a priori comparisons between the exact terms computed from the DNS and their modeled counterparts.

## 2 Governing Equations and Numerical Method

Dense gas flows are governed by the compressible Navier-Stokes equations, supplemented by suitable thermodynamic and transport-property models. In the present work, the gas behavior is modeled through the Martin–Hou (MAH) thermal equation of state [5], which is reasonably accurate for the fluid of interest and requires a minimum amount of experimental information for setting the gas-dependent coefficients. In addition thermodynamic models relating the dynamic viscosity $\mu$ and thermal conductivity $\kappa$ to the gas temperature and pressure have to be specified. In the present calculations, the transport properties follow the Chung et al. model [6], which incorporates a correction term in the dense-gas region. The working fluid is perfluoro-perhydrophenanthrene (chemical formula $C_{14}F_{24}$), called hereafter with its commercial name PP11, often used in dense-gas studies. DNS were also carried for air, modeled as a polytropic perfect gas. In the latter case, the viscosity is assumed to follow a power law of the temperature and the thermal conductivity is computed according to a constant Prandtl number assumption. The governing equations are approximated in space by means of optimized finite difference schemes, supplemented by an optimized selective sixth-order filter. A low-storage six-step optimized Runge-Kutta is used for time integration.

## 3 DNS results

A parametric study was carried out at three bulk Reynolds numbers $Re_B := \frac{\overline{\rho}_B \widetilde{u}_B h}{\overline{\mu}_w}$ (3000, 7000 and 12000) and three bulk Mach numbers $M_B := \frac{\widetilde{u}_B}{\overline{c}_w}$ (1.5, 2.25 and 3.0) [4]. Details about the computational setup and grid resolution can be found in [4]. In the following, the subscripts $(\cdot)_B$, $(\cdot)_w$ and $(\cdot)_{CL}$ denote time and space averaged values over the channel cross-section, at the wall and at the centerline, respectively; $\overline{(\cdot)}$ indicates Reynolds averaging and $(\cdot)'$ Reynolds fluctuations; similarly, $\widetilde{(\cdot)}$ and $(\cdot)''$ denote Favre averages and fluctuations. Results for the different cases were compared by introducing an empirical semi-local scaling initially proposed by Huang et al. [7] for compressible flows, which corrects the usual wall scaling with centerline quantities. Specifically, $y^* = \frac{\overline{\rho}(y) u_\tau^* y}{\overline{\mu}(y)}$ and $Re_\tau^* = Re_\tau \sqrt{\frac{\overline{\rho}(y)}{\overline{\rho}_w}} \frac{\overline{\mu}_w}{\overline{\mu}(y)}$, with $u_\tau^* := \sqrt{\frac{\overline{\tau}_w}{\overline{\rho}(y)}}$ the semi-local friction velocity. This mixed scaling provided quite satisfactory results in collapsing first- and second-order moments for a wide range of $M_B$. For PP11, due to the large specific heat of the fluid, the average temperature is almost constant across the channel for any choice of the Mach and Reynolds numbers, and the centerline temperature differs less than 1% from $\widetilde{T}_w$. Decoupling of dynamic and thermal effects in the dense gas also leads to smaller mean density variations across

the channel. The normalized viscosity $\overline{\mu}/\overline{\mu}_w$, which follows temperature variations for air, varies instead like the density for PP11 and tends to decrease toward the channel center. As a consequence the friction Reynolds number $Re_\tau^*$ increases toward the channel centerline in PP11. Specifically, the dense gas flow exhibits lower values of $Re_\tau^*$ near the wall, compared to a perfect gas flow at the same bulk conditions, whereas the centerline value of $Re_\tau^*$ is much higher in the dense gas, due to the negligible friction heating in the outer region. On the other hand, the average Prandtl number $\overline{Pr}$ decreases from the wall to the centerline, following essentially the same trend as the average specific heat. Figure 1 displays the distributions of the above-mentioned quantities across the channel, as a function of $y^*$. Dense gas effects are stronger at higher $M_B$, since the local thermodynamic states spread over a wider range. Sample results for second-order statistics are reported in figure 2, which displays the r.m.s. values of the density, the Reynolds shear stress in semi-local scaling $\overline{\rho u'' v''}^+ = \tau_w^{-1}\overline{\rho u'' v''}$, as well as the ratio of the turbulent kinetic energy production to dissipation. The relative density and pressure fluctuations are of the same order of those observed for air flows (see [4]), whereas temperature fluctuations (not reported) are nearly two orders of magnitude lower. Remarkably, $\overline{\rho'^2}$ decreases monotonically from wall to centerline, contrary to light gases. This is due to the peculiar thermodynamic behavior of PP11 at the considered conditions, as demonstrated in [4] by using the equation of state. In all cases, density fluctuations remain small compared to the mean value, and Morkovin's hypotesis is satisfied even at the highest Mach number. Despite the striking differences in the thermodynamic behavior, Reynolds stress profiles are similar to those observed, e.g., in [8] for low-Mach TCF with temperature-dependent transport properties. The liquid-like behavior of viscosity leads to an increase of the spanwise, wall-normal and Reynolds shear stresses with respect to the corresponding incompressible evolution, whereas the streamwise one decreases. This effect is stronger when increasing Mach number. The last subfigure shows the ratio of production to dissipation term $P_k/\varepsilon_k$ of the turbulent kinetic energy budget. The production peak is located as usual at $y^* \approx 12$. For the higher Reynolds number, a second production peak is observed in the outer region, like in high-$Re$ incompressible flow, due to the reduced dissipation close to centerline. A visualization of flow structures for $M_B = 3$, $Re_B = 12000$ is provided in figure 3.

## 4 A priori analysis of turbulence models

DNS data are used to investigate the validity of some popular models for the RANS equations. More specifically, we focus hereafter on the eddy-viscosity and turbulent Prandtl number assumptions, commonly used to approximate, respectively, the Reynolds stress tensor and the turbulent heat flux. To this end, "exact" eddy viscosity and turbulent Prandtl number are computed from DNS data as:

$$\mu_t = \overline{\rho u'' v''} \left( \frac{d\overline{u}}{dy} \right)^{-1} ; \quad Pr_t = \overline{c}_p \mu_t / \lambda_t \tag{1}$$

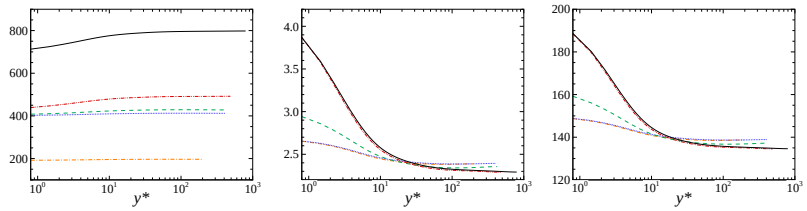


| | | | | | |
|---|---|---|---|---|---|
| $M_B$ | 1.5 | 1.5 | 2.25 | 3 | 3 |
| $Re_B$ | 3000 | 7000 | 7000 | 7000 | 12000 |
| Line | -·-·- | ····· | – – – | -··-··- | ——— |

**Fig. 1** From left to right: local friction Reynolds number ($Re^*_\tau$), average Prandtl number ($\overline{Pr}$), and average isobaric specific heat normalized with the gas constant ($\overline{c}_p/R$) as a function of $y^*$ for DNS of PP11 TCF at various $M_B$ and $Re_B$.

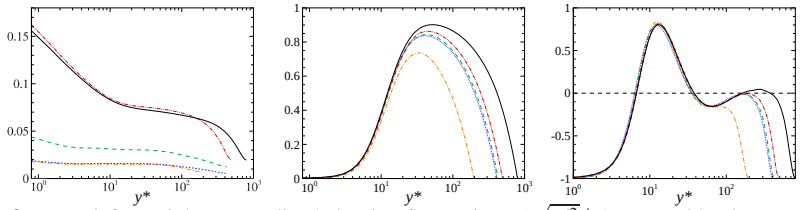


**Fig. 2** From left to right: normalized density fluctuations ($\sqrt{\overline{\rho'^2}}/\overline{\rho}$), Reynolds shear stresses ($\overline{\rho u'' v''}^+$), and production-to-dissipation ratio of turbulent kinetic energy ($P_k/\varepsilon_k - 1$) as a function of $y^*$ for DNS of PP11 TCF at various $M_B$ and $Re_B$. Line legend as in figure 1

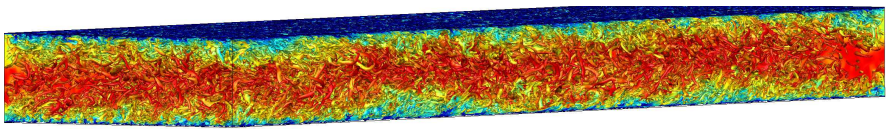

**Fig. 3** Isosurface of $Q(h/u_B)^2 = 1$ coloured with streamwise velocity ($M_B$=3, $Re_B$=7000).

where $\overline{u}$ is the average streamwise velocity and $\lambda_t = \overline{\rho v'' h''} \left(\frac{d\overline{h}}{dy}\right)^{-1}$ is a turbulent thermal conductivity, with $\overline{h}$ the average static enthalpy. Input quantities required by eddy models are also based on DNS. In this study we restrict our attention to two low-Reynolds variants of the $k-\varepsilon$ model, namely, the Launder–Sharma (LS) [11] and Chien (CH) [12] models, which assume that $\mu_t = C_\mu f_\mu \rho k^2/\varepsilon$, with $C_\mu$ usually taken equal to 0.09, the damping function $f_\mu$ is $\exp(-3.4/(1+R_t/50)^2)$ ($R_t = \rho k^2/(\mu\varepsilon)$) for LS and $1-\exp(-0.0115y^+)$ for CH. Durbin [10] showed that a more appropriate choice for the velocity scale in the inner region is represented by the root-mean square of the wall-normal fluctuating velocity, and reformulated the eddy viscosity as $\mu_t = C\sqrt{\widetilde{v''^2}}k/\varepsilon$ with $C = 0.2$. In figure 4 we report the results for the highest Reynolds number, both for air and PP11. In both cases the LS model badly overestimates the turbulent viscosity, especially in the viscous sublayer, as also observed by other authors (e.g. [10]) for incompressible flows. Chien's model captures better the trend of $\mu_t$ but also overestimates the turbulent viscosity in the outer region. Durbin's model provides a reasonably accurate approximation of the

$\mu_t$ profile up to part of the logarithmic region. For air, the model departs from the DNS profile at $y^* \approx 40$ and, unlike the two preceding models, it underestimates $\mu_t$ in the outer region. For PP11, the model remains in rather good agreement with DNS up to $y^* \approx 150$ and overestimates $\mu_t$ for higher values of $y^*$.

In figure 5 we report the exact turbulent Prandtl number at various $M_B$ and $Re_B$. For air, $Pr_t$ follows the trends observed by other authors in the literature (e.g. [7]). In particular, for the present relatively low-Re flow, $Pr_t$ exhibits only a small plateau around $y^* \approx 100$ where its value is close to the standard "constant" value of 0.9. In the outer region, $Pr_t$ decreases with $y^*$, while in the inner region it exhibits a local maximum at about $y^* = 50$ and tends to approximately 1.1 at the wall. For PP11, the overall behavior is rather close to that of the perfect gas over most of the channel height ($y^* \gtrapprox 5$). However, the solution exhibits a larger '0.9' plateau than the air flow, located at $y^* \approx 120$, most likely because of the higher local $Re^*_\tau$. The local maximum around $y^* \approx 50$ is also observed for the dense gas. A drastically different behavior is observed in the viscous sublayer ($y^* \lessapprox 5$), where the local Prandtl number is much higher and the local $Re^*_\tau$ much lower than in air. In this region ($y^* \approx 2$), $Pr_t$ exhibit another local maximum (more or less pronounced according to the flow conditions) and tends to values lower than 1 at the wall ($\approx 0.4$ at the highest Mach number). Inspection of the DNS data for $\mu_t$ and $\lambda_t$ suggests the following explanation: for air, both $\mu_t$ and $\lambda_t$ decrease approximately at the same rate ($O(y^{*3})$) when $y^* \to 0$. Since in this case $c_p = const$, then $Pr_t$ tends toward a constant nonzero value. For PP11, $\lambda_t$ decreases at a lower rate than $\mu_t$ in the near wall region, due to the smaller enthalpy variation in this high-$c_p$ fluid. As a consequence, their ratio tends to vanish at the wall. However, $\overline{c}_p$ increases abruptly when $y^* \to 0$ (following an approximately exponential trend), hence the local maximum.

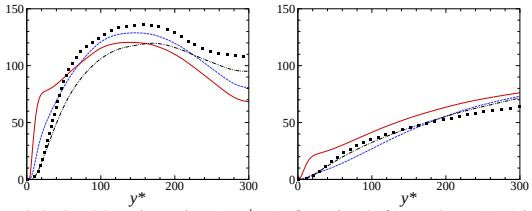


**Fig. 4** Exact and modeled eddy viscosity ($\nu_t/\nu_w$) for air (left) and PP11 (right) at $M_B = 3$ and $Re_B = 12000$. ——: LS; – – –: CH; – · – · –: Durbin; ■: DNS.

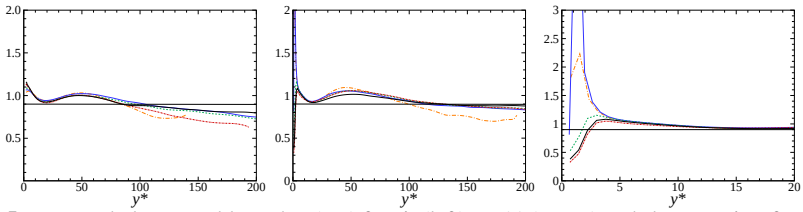


**Fig. 5** Exact turbulent Prandtl number ($Pr_t$) for air (left), PP11 (centre) and close-up view for PP11 (right) at various $M_B$ and $Re_B$. Legend as in figure 1. Horizontal line is set at $Pr_t = 0.9$.

## 5 Conclusions

Direct numerical simulations of plane turbulent channel flows of dense gases have been performed at various bulk Mach and Reynolds numbers. For a dense-gas, the classical $y^+$ scaling based on the friction velocity fails to collapse thermodynamic profiles and Reynolds stresses at high $M_B$, and semi-local scaling, which accounts for variations of the flow properties, has to be adopted instead. Due to the high specific heat, coupling between dynamic and thermal effects is found to be very small for the dense fluid. Turbulence structure is shown to be little affected by dense gas effects. For the adopted thermodynamic conditions, transport properties exhibit a liquid-like behavior and the local Reynolds number in the outer region is found to be much higher than in corresponding air flows. A priori analyses of the validity of some common modeling assumptions for the eddy viscosity and turbulent Prandtl number showed that, for a dense gas, turbulence models for eddy viscosity follow the exact trend more closely than in perfect gas (at the present high Mach numbers), due to the higher local Reynolds number, but eddy viscosity is overestimated. An adjustment of the model constant could help improving the results. A peculiar behavior is observed for the turbulent Prandtl number close to the wall, which peaks more or less abruptely in the viscous sublayer, instead of tending to a constant value. Further investigations of the near wall thermal behavior are planned as future research.

**Acknowledgements** This work was granted access to the HPC resources of GENCI (Grand Equipement National de Calcul Intensif) under the allocation 7332.

## References

1. Thompson,P.A.: A fundamental derivative in gasdynamics. Phys. Fluids **14**, 1843–49 (1979).
2. Sciacovelli, L., Cinnella, P., Content, C., Grasso, F.: Dense gas effects in inviscid homogeneous isotropic turbulence. J. Fluid Mech. **800** 140–179 (2016).
3. Sciacovelli, L., Cinnella, P., Grasso, F.: Small-scale dynamics of dense gas compressible homogeneous isotropic turbulence. J. Fluid Mech. (2017). In press.
4. Sciacovelli, L., Cinnella, P., Gloerfelt, X.: DNS of supersonic turbulent channel flows of dense gases. J. Fluid Mech. **821** 153–199 (2017).
5. Martin, J., Hou, Y.: Development of an equation of state for gases. AIChE J. **1**,142-151 (1955).
6. Chung, T.H., Ajlan, M., Lee, L.L., Starling, K.E.: Applications of kinetic gas theories and multiparameter correlation for prediction of dilute gas viscosity and thermal conductivity. Ind. Eng. Chem. Res. **27**, 671–679 (1988).
7. Huang, P.G., Coleman, G.N., Bradshaw, P.: Compressible turbulent channel flows: DNS results and modeling. J. Fluid Mech. **305**, 185–218 (1995).
8. Patel, A., Peeters, J.W.R., Boersma, B.J., Pecnik, R.: Semi-local scaling and turbulence modulation in variable property turbulent channel flows. Phys. Fluids **27**, 095101 (2015).
9. Shih, T.H.: An improved $k-\varepsilon$ model for near-wall turbulence and comparison with direct numerical simulation. NASA TM 103221 (1990).
10. Durbin, P.A.: Near-Wall turbulence closure modeling without ”damping functions”. Theoret. Comput. Fluid Dynamics **3**, 1–13 (1991).
11. Launder, B.E., Sharma, B.I.: Application of the energy-dissipation model of turbulence to the calculation of flow near a spinning disc. Lett. Heat Mass Transf. **1**, 131–138 (1971).
12. Chien, K.Y.: Predictions of channel and boundary-layer flow with a low-Reynolds turbulence model. AIAA J. **20**, 33–38 (1982).